
Research into the Physical Mechanism of Erosion

Studies of processes occurring between the particles and target surface involved the following problems:

- 1) Macro- and microgeometry of a wearing surface;
- 2) Stress distribution and structural changes in the target surface layer;
- 3) Fragmentation of abrasive particles and adhesion of the latter to the surface.

2.1 Changes in the Macro- and Microgeometry of a Wearing Surface

In the process of erosion, changes take place both in the micro- and macrogeometry of a wearing part. From the examples given in Figure 2.1, it is obvious that these changes are also accompanied by changes in the parameters of wear (especially the impact angle). The surface is subject to gradual formation of ripples as described in Section 1.7 above.

Changes occurring in the microgeometry caused by particle impacts have been studied in relation to explaining the physical mechanism of erosion. Depending on the impact angle, properties of the material and particle shape, impact scars appearing in the surface were found to vary in shape as well. Several authors have analyzed traces of impact emerging on the previously polished – and sometimes subsequently etched – metal bodies. Those studies were carried out throughout the 1960s and 1970s [1–5]. Typical impact craters brought about by normal impact ($\alpha = 90^\circ$) are shown in Figure 2.2.

Figure 2.2a,c shows the emergence of block-shaped formations around the impact crater brought about by shearing deformations of cobalt, whereas the trace of impact on the surface of brittle tungsten is surrounded by radial cracks (Figure 2.2b). At a moderate impact velocity ($v_0 = 50$ m/s), the trace in the surface of plastic steel – with its clear-cut outline – resembles the indentation typical for Brinell hardness test (Figure 2.2d); the impact crater obtained at high velocity (Figure 2.2e), however, is surrounded by a ridge of sparse metal which consists of the material squeezed out as a result of shear strain.

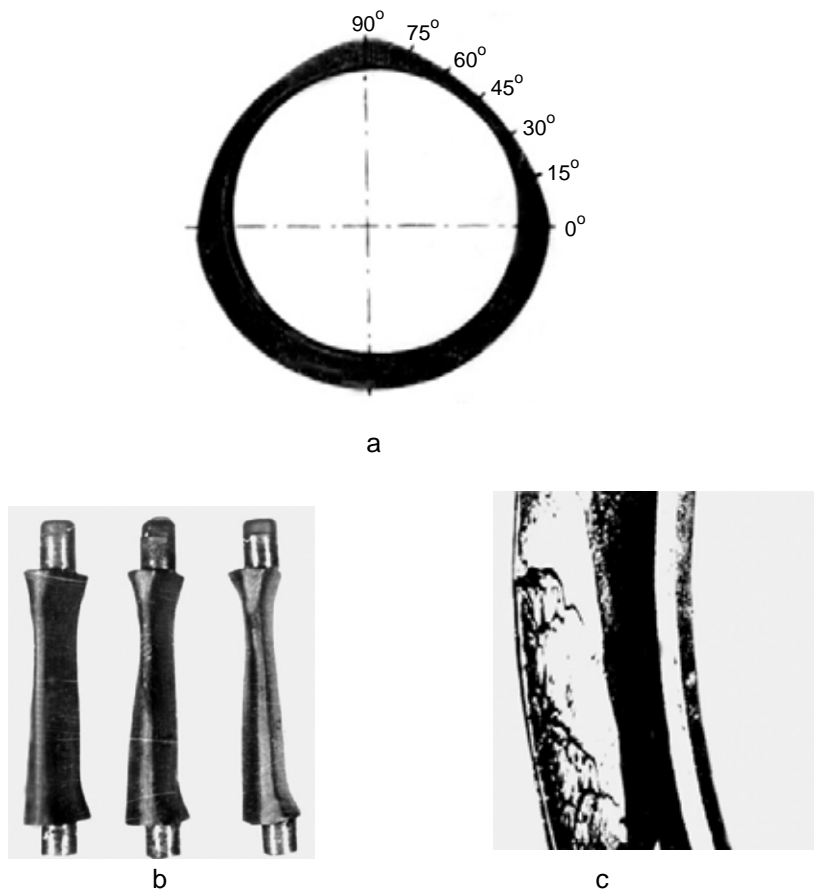


Figure 2.1a–c. Examples of changes in the macrogeometry of the component: **a** – cross-section the boiler tube, subject to fly ash erosion; **b** – gradual changes in the shape of cylindrical disintegrator pin used for grinding sand-lime mixture; **c** – surface ripples emerging in the pipe elbow used for pneumotransport (upward stream direction)

Figure 2.3 shows impact traces if $\alpha < 90^\circ$. In this case, the material excluded from the impact trace is submitted to directed shear strain. Depending on the value of α , particle size and its position at the moment of hitting the surface, the shape of the trace can vary. Thus, the material squeezed out from the crater may become pressed to the front and the sides of the impact scar (Figure 2.3b), or form a lip the front of it (Figure 2.3d,f), without any material removal from the surface. Alternatively, the particle may remove the whole volume of material out of the crater at the first impact already (Figure 2.3a,c). Systematic research with analogous results has also been carried out by scientists from Cambridge University [6, 7].

As far as ductile materials are concerned, wear rate in the initial stage of the process is generally lower than in permanent conditions, because only a little piece of crater volume material is removed. In order to study the ratio between the

volume of impact craters and the material removed, single craters in the polished surfaces of test pieces were studied by means of a measuring microscope and profilometer [2]. Using the symbols in Figure 2.4, Table 2.1 presents the results obtained at low impact angles.

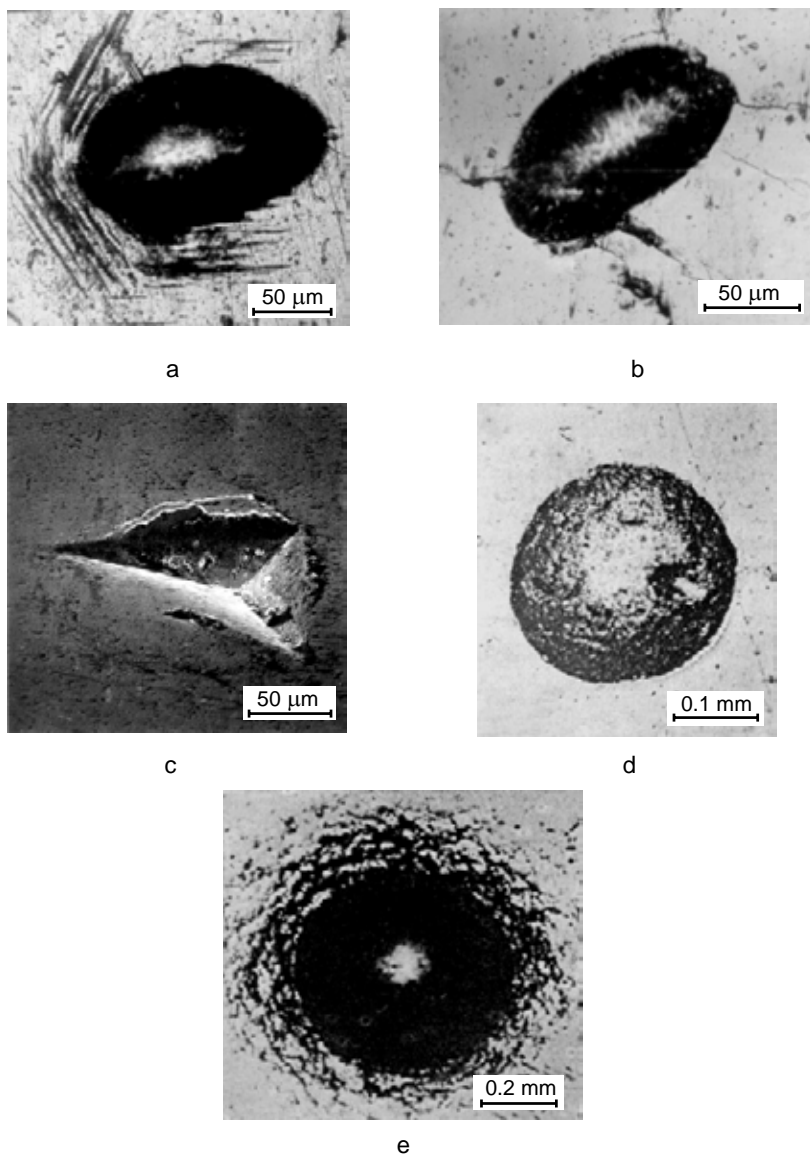


Figure 2.2a-e. Impact craters produced by particles hitting the metal surface at $\alpha = 90^\circ$: **a** – impact of particles of sand of 0.4–0.6 mm on a cobalt target, $v_0 = 80$ m/s; **b** – the same as “a” but on a tungsten surface; **c** – impact of 0.6–0.8 mm particle on a WC-6Co hardmetal surface, $v_0 = 225$ m/s; **d** – impact crater produced by a 0.9 mm spherical cast iron pellet on the 0.2% C steel target surface, $v_0 = 50$ m/s; **e** – the same as “d”, $v_0 = 225$ m/s

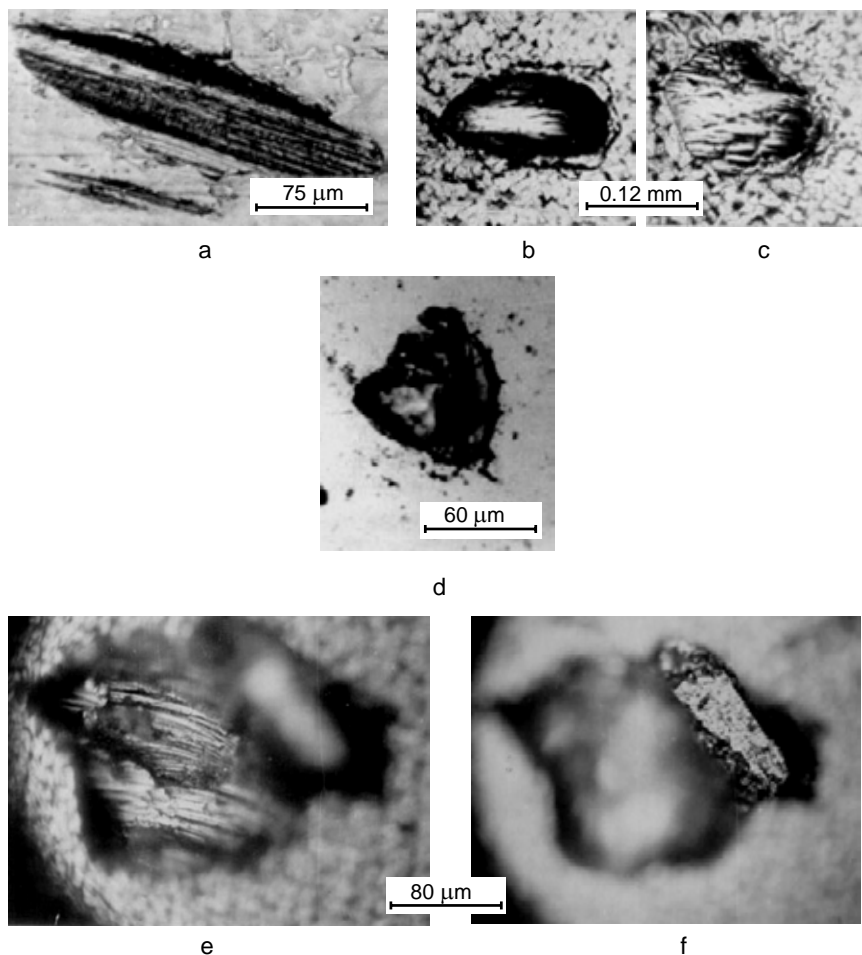


Figure 2.3a-f. Impact craters produced by particles hitting metal surface at $\alpha < 90^\circ$, with the velocity vector directed from left to right: **a** – craters of 0.4–0.6 mm particles of sand from the Männiku quarry on the surface of 0.2% C steel, $\alpha = 3^\circ$, $v_0 = 100$ m/s; **b** – craters of 0.3–0.4 mm particles of sand from the Männiku quarry on 0.2% C steel, $\alpha = 30^\circ$, $v_0 = 150$ m/s; **c** – the same as “b”; **d** – impact scar left by 0.3–0.4 mm particle from the Männiku quarry on the hardened steel 710 HV, $\alpha = 45^\circ$, $v_0 = 80$ m/s; **e, f** – scars of 0.3–0.4 mm particle of sand from the Männiku quarry on the surface of 0.2% C steel, $\alpha = 40^\circ$, $v_0 = 150$ m/s; **e** – focused on the bottom of the crater; **f** – focused on the squeezed-out lip

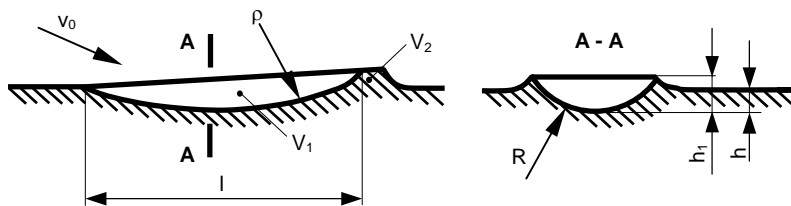


Figure 2.4. Scheme of impact crater at low impact angles: V_1 – volume of impact crater, V_2 – volume of material ousted from the surface but not separated from it

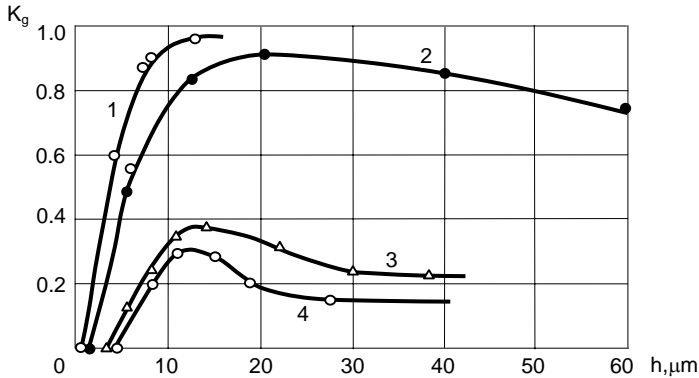
Table 2.1. Data on impact craters in 0.2% C steel target surface eroded by 0.4–0.6 mm quartz sand from the Männiku quarry, $v_0 = 97$ m/s

α°	$l, \mu\text{m}$	$h, \mu\text{m}$	$\rho, \mu\text{m}$	$V_1, \mu\text{m}^3 \times 10^{-3}$	$V_2, \mu\text{m}^3 \times 10^{-3}$	$K_g = \frac{(V_1 - V_2)}{V_1}$	$Z, \%$	K_g'
3	197	3	1618	6.7	3.4	0.49	100	0.49
9	136	4	580	12.2	7.9	0.35	93	0.36
15	136	7.6	308	29.8	21.4	0.28	73	0.35
30	126	10.3	192	46.4	38.7	0.17	53	0.26

Note: 1) In each regime, at least 15 craters were measured whereas the table gives mean results

2) Z shows the percentage of the impact craters from which material was removed and K'_g , in contrast to K_g , takes into account only those scars where it occurred

Analogous tests on hardened steel indicated that the values of ratio K_g were considerably higher than those of ductile steel [1]. This correlates with the test results obtained in scratching various metals [8] with a diamond bit ($R = 49 \mu\text{m}$). Curves in Figure 2.5 demonstrate the corresponding test results.

**Figure 2.5.** Dependence of ratio K_g on the depth of the scratch h : 1 – for hardened steel, 2 – for cast iron, 3 – for annealed steel and 4 – for copper

At single impact – as shown above – the shapes of the craters left in the surface by impacting particles vary considerably in their shape, whereas, when the craters overlap (*i.e.* in the permanent phase of the wear), the microgeometry of the surface at different angles is quite similar (Figure 2.6a,b). So are the shapes of the wear particles (except when $\alpha = 3^\circ$; see Figure 2.7a, in which the shape resembling that of a microchip prevails). In the case of hardmetals, wear-out of the binder from between the carbide grains, revealing grains of carbide, occurs quite often (Figure 2.6c) and is rather independent of the impact angle.

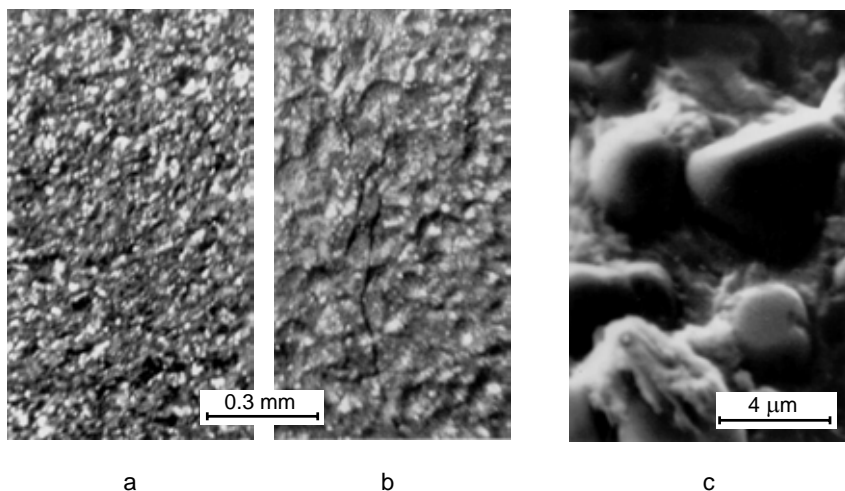


Figure 2.6a-c. Microgeometry of eroded surfaces: **a** – steel 0.2% C, $v_0 = 50$ m/s, $\alpha = 30^\circ$, 0.4–0.6 mm corundum; **b** – the same as “a”, $\alpha = 90^\circ$; **c** – TiC-Ni-Co cermet, $v_0 = 80$ m/s, $\alpha = 90^\circ$, iron scale 0.1–0.3 mm

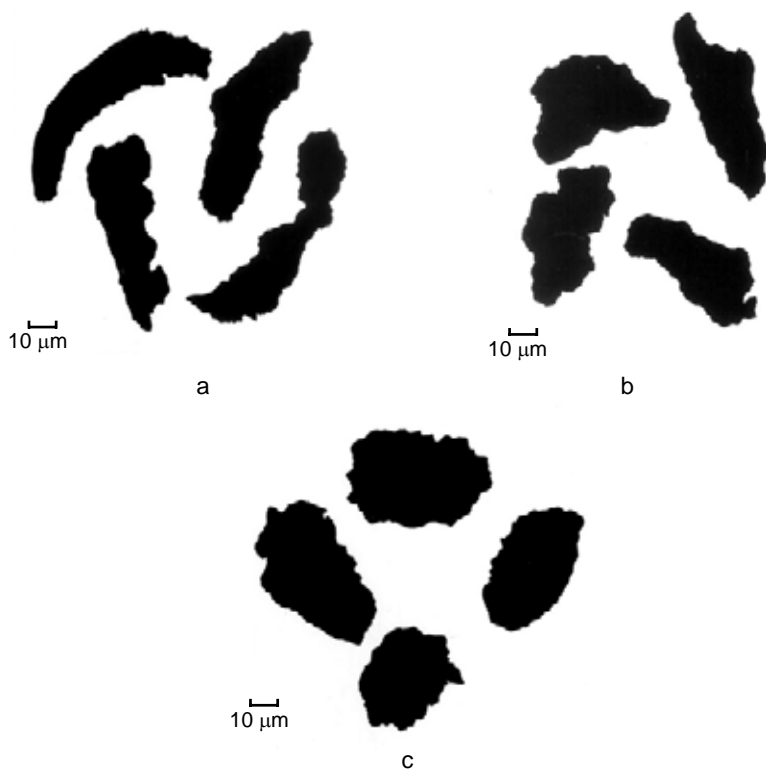


Figure 2.7a-c. Typical copper wear debris (enlarged), $v_0 = 130$ m/s, corundum particles 0.3–0.4 mm: **a** – at $\alpha = 3^\circ$, **b** – at $\alpha = 15^\circ$, **c** – at $\alpha = 90^\circ$

2.2 Stress Distribution and Structural Changes in Target Material Surface Layer

Ductile metals attacked by a stream of hard particles are subject to strain hardening of the surface accompanied by higher hardness and emergence of residual compressive stresses in the surface layer – an effect used in shot peening processes to increase the fatigue resistance of a metal [9]. The values of surface hardness obtained in the process of shot peening vs layer thickness are presented in Figure 2.8a. A picture similar to that will be obtained for the case of erosion by sand particles (Figure 2.8b).

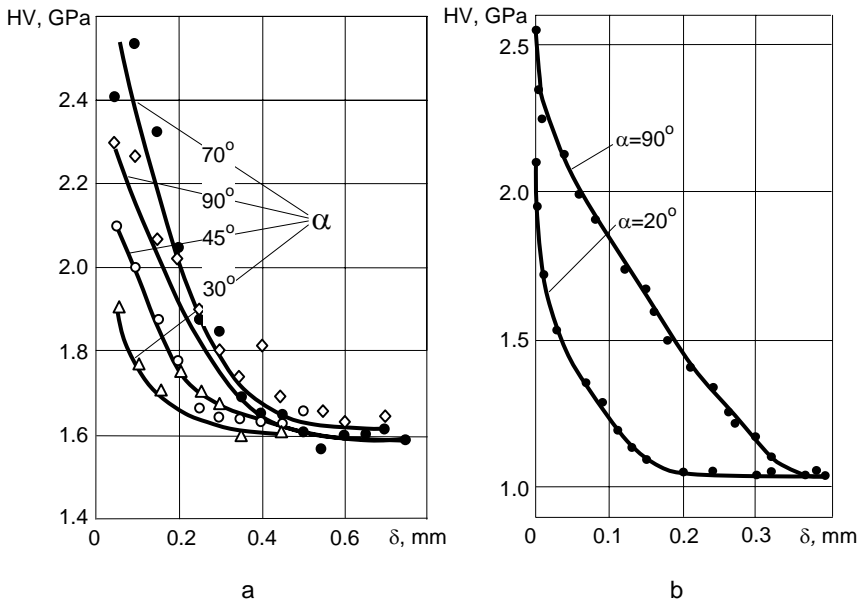


Figure 2.8a,b. Hardening – as a result of surface strain hardening – within the layer at various values of depth δ : **a** – 0.3% C steel, cast iron pellets of 1–1.5 mm are accelerated by an air stream under the pressure of 0.5 MPa [9]; **b** – Armco-iron in a stream of 0.4–0.6 mm quartz sand, $v_0 = 80$ m/s [4]

X-ray examination resulted in a similar picture of processes taking place in the surface layer. The first studies of this kind were carried out on specimens of 0.2% C steel subjected to stress relief annealing at 650 °C prior to the test [10]. The test specimens were eroded with 0.3–0.6 mm quartz sand from the Männiku quarry, using the CAK-1 testing facility at the velocity of $v_0 = 80$ m/s. Widening of interference lines on Debye-Sherrer diagrams was recorded by the X-ray defectoscope, gradually increasing the amount of sand hitting the test piece (Figure 2.9a). After that, part of the strain hardened layer was peeled off little by little by electric polishing, and relative widening of X-ray lines was determined (Figure 2.9b). It is obvious that these curves rather closely resemble those in Figure 2.8 obtained by measuring microhardness. It follows from Figure 2.9a that a permanent wear regime arrives after 1 cm² of the surface of the test piece has been hit by 20 g of sand because, thereafter, the X-ray lines become stable. On

the basis of Figure 2.9b it can be concluded that, in this case, the strain hardened layer is 0.25–0.3 mm thick. The same operations performed at $\alpha = 20^\circ$ led to stable X-ray lines after hitting the surface by 15 g/cm² of sand and the thickness of the strain hardened layer was recorded to be 0.15–0.2 mm.

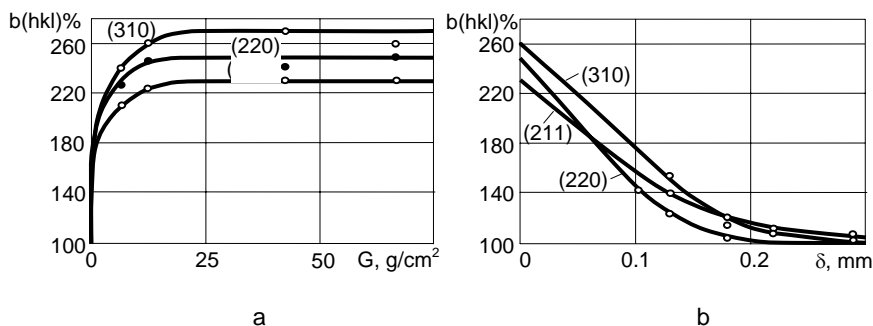


Figure 2.9a,b. X-ray studies on eroded mild steel specimens in a stream of quartz sand, $v_0 = 80$ m/s: **a** – relative change in the width of X-ray lines b depending on the mass of abrasive hitting the test body, $\alpha = 90^\circ$; **b** – relative change in the width of X-ray lines b depending on the thickness of the strain hardened layer δ removed in the process of electrolytical polishing

Pakkas widened the range of the impact velocities at tests on mild steel as high as 195 m/s [11]. The relative widening of X-ray lines range in his work as presented in Figure 2.10.

For 0.2% C steel, analysis of the shape of X-ray lines according to Warren was carried out to determine the dependence of lattice distortion on particle velocity [5]. The range of 50–225 m/s was studied at an impact angle of 90° . Test pieces were eroded by quartz sand and cast iron pellets of 0.4–0.6 mm size. In both cases curves were obtained, with the clear-cut maximum at $v_0 = 120$ m/s. In view of the results of both microhardness and X-ray tests, it may be interesting to add that maximum distortion in crystallic lattice and maximum degree of strain hardening do not occur at the impact angle of 90° but in the range of 70 – 75° , instead.

To observe processes taking place in the surface layer, microsections of worn specimens were made transverse to the surface and examined under a microscope. Photos obtained with ductile metals, like those reported by several other researchers, show grain distortions in crystal texture and cracks running along the surface (example in Figure 2.11a).

In the microsections of hardened steel, however, white non-etchable layers of 1–2 μm thickness (Figure 2.11b) appeared, which run nearly along the equipotential lines of maximum shear strains [1]. Inasmuch as the layers are very thin, it is difficult to determine their composition – but in most cases they are treated as secondary martensite [12]. It is noteworthy, however, that at normal impact removal of the wear debris takes place along those white layers (see Figure 2.11c). A parameter closely related to the above phenomena is rise in temperature, accompanying the impact of the particles. The latter is confirmed by a number of researchers who have measured the instantaneous temperature rise both on the impact of particles and in the process of metal grinding. Similarity between thermal processes taking place on erosion (especially at low impact angles) and in the process of grinding, is also testified by the fact that in both cases flying sparks occur.

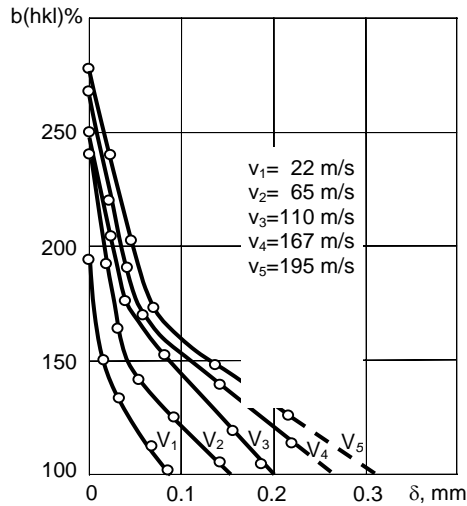


Figure 2.10. Dependence of relative widening of X-ray line (220) on the thickness of the layer removed by electrolytical polishing, $\alpha = 90^\circ$

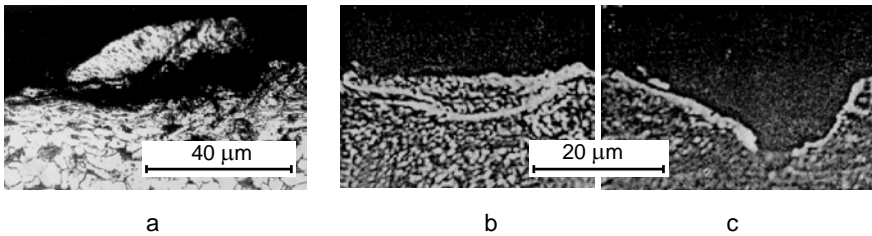


Figure 2.11a–c. Samples of microsections made perpendicularly to the worn surface: **a** – 0.2% C steel, $v_0 = 80$ m/s, $\alpha = 45^\circ$, quartz sand 0.3–0.6 mm; **b,c** – 0.8% C hardened steel, $v_0 = 80$ m/s, $\alpha = 90^\circ$, quartz sand 0.6–1 mm, **b** – without separation of wear debris, **c** – with separation of wear debris

Luminescence of the sample in the zone of bombardment by ash particles at velocities ranging from 200 to 300 m/s was described by Olesevich [13]. He considered that in the contact zone heating of one or both colliding bodies occurs to a temperature that corresponds to light yellow luminescence, the intensity of which depends on the impact intensity.

Uetz and Gommel [14] measured the temperature during the impact of steel pellets (790 HV) against a steel plate (190 HV). At an impact velocity of 70 m/s, the maximum temperature measured was 510 °C. The real surface temperature is assumed to be higher than that measured.

Polosatkin and Griбанov [15] used the thermocouple method in conjunction with scratching to measure the temperatures involved. Scratch velocities were in the range of 1–800 m/s. The melting temperatures on the surfaces of all metals tested were measured at scratch velocities exceeding 250 m/s.

Using a scanning electron microscope and a microanalyser, thermal processes accompanying erosion and grinding were studied in collaboration with researchers from the University of Stuttgart [16]. First, specimens of hardmetals

and steel were eroded at high impact velocities in which small spheres were detected in their surface layer (Figure 2.12). Analysis performed with a microanalyser indicated that the chemical composition of the small balls corresponds to that of the basic material. Among the products of grinding and also those flying off as sparks, analogous small balls were found both apart from and adhered to the microchips (Figure 2.13). Alternatively, combinations of molten metal may adhere to the abrasive grains of the grinding wheel (Figure 2.13e,f). The photo of broken pellets proves that they are of hollow shape (Figure 2.13b).

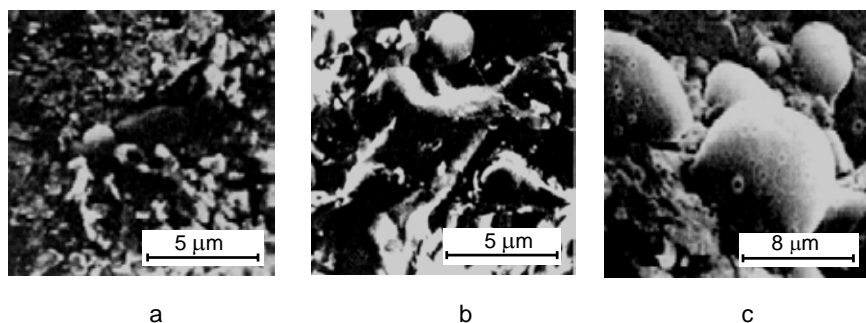


Figure 2.12a–c. Spherical particles on the surface: **a** – on the surface of WC-Co hardmetal, $v_0 = 325$ m/s, $\alpha = 90^\circ$, abrasive-cast iron pellets 0.4–0.6 mm; **b** – the same on the surface of chromium carbide based cermet, $v_0 = 325$ m/s, $\alpha = 90^\circ$, abrasive quartz sand 0.4–0.6 mm; **c** – the same on the surface of 0.45% C steel, $v_0 = 108$ m/s, $\alpha = 60^\circ$, abrasive quartz sand 0.4–0.6 mm

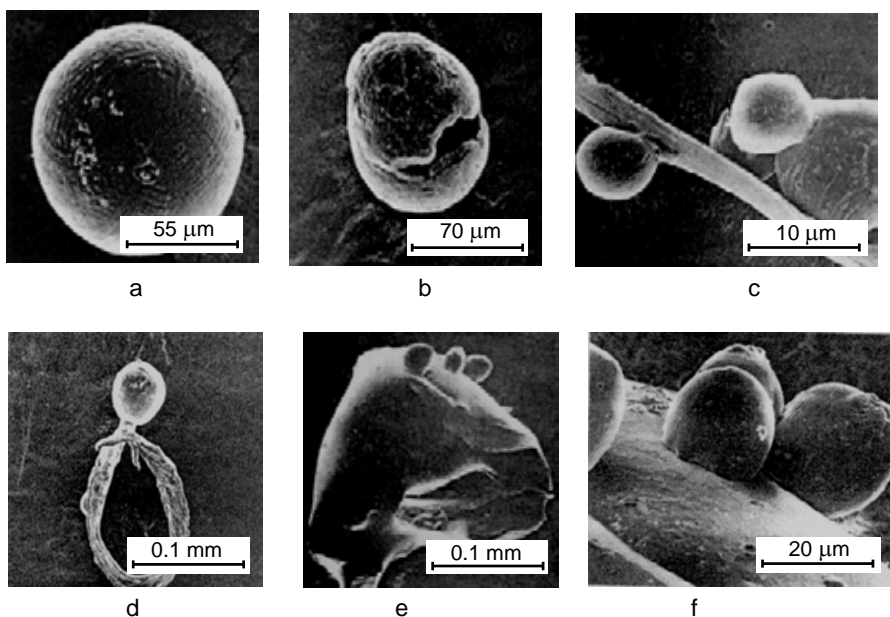


Figure 2.13a–f. Spherical particle formed in grinding: **a** – in grinding of cobalt, $v_{grind} = 35$ m/s; **b** – the same formed in grinding of 0.45% C steel; **c** – spherical particles of 0.45% C steel melted (agglomerated) into a group, $v_{grind} = 35$ m/s; **d** – the same as “b”; **e,f** – spherical particles of 0.45% C steel on the grain surface of a grinding wheel, $v_{grind} = 35$ m/s

From experimental evidence, melting temperatures can be attained in microvolumes during abrasive wear, *i.e.* abrasive erosion at velocities ranging from 100 to 325 m/s and grinding at a velocity of 30 m/s. Hence, during abrasive erosion, the microvolumes of a material heated to a high temperature in the impact zone may be thrown out in the shape of microdroplets. These microdroplets are shaped into spheres by the action of surface tension. The formation of spherical particles in grinding takes place in an identical manner.

When abrasive grains contact metal surfaces, depending of their orientation and pressure, a number of the microvolumes of ground material become liquid because of the local high temperatures involved and are scattered into the surrounding space. The sparks appearing in grinding, as well as in abrasive erosion, are glowing spheres.

In abrasive erosion it can be assumed that the majority of the spherical particles are scattered and lost and only a small number remain on the surface of the sample where they can be detected. The detection of spherical particles in abrasive erosion is evidence that in this wear mode thermal factors as well as mechanical factors are involved in breaking up the thin surface layers of the material. Although the quantity of spherical particles formed in the wear process is large, their specific weight in the wear product from abrasive erosion up to a velocity of 325 m/s is negligible. The preliminary evaluation of the role played by the thermal factor, *i.e.* the content of spherical particles in the total volume of the product is higher in grinding than in abrasive erosion.

2.3 Fragmentation of Abrasive Particles and Adhesion of the Latter to the Surface

One of the phenomena accompanying abrasive erosion is the fragmentation of abrasive particles. For this, depending on particle composition and initial defects, the respective critical impact velocity shall be obtained. Three different zones are distinguished in a fracturing particle at sufficiently high impact velocity [17] (Figure 1.16): the powdered lower cone, whose fragments at velocity $v_T > v_0$ are projected away along the surface; the non-destructed residual cone and the bigger orange-peel shaped splinters. The lower cone increases and the upper one decreases with an increase in the impact velocity. It is important to know all the parameters influencing the process of effective size reduction in the impact milling equipment. The milling effect is estimated quantitatively by the increase of particle specific surface ΔS (m^2/kg), using the corresponding testing equipment. The problems related to milling have been dealt with by Piel [18], and more profoundly analyzed by Kleis and Uuemõis in their monograph [19]. The main results obtained on the vacuum device VK-2 are referred to hereinafter.

Similarly to the equation $I_g = C_1 \cdot v^m$, demonstrating the relationship between the wear rate I_g and impact velocity v_0 , the increase of the specific surface can be expressed through the exponential function

$$\Delta S = C_2 v^n. \quad (2.1)$$

An example of the experimental results is given in Figure 2.14a. Impact angle α and hardness of impact surface H are also important parameters. The maximum

fragmentation effect takes place at $\alpha = 90^\circ$ and the curves $\Delta S = f(HV)$ are stabilized when the hardness of the impact surface exceeds that of the fractured particle (Figure 2.14b).

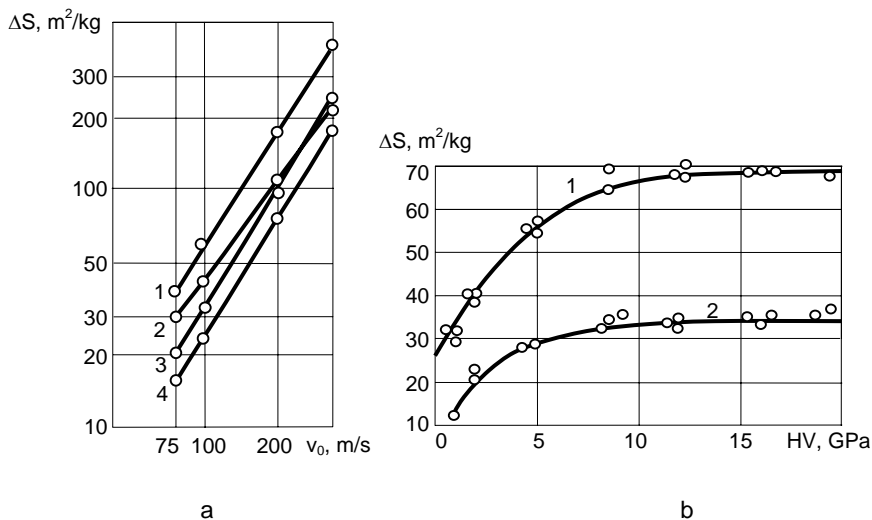


Figure. 2.14a,b. Dependence of increase in the specific surface of 0.4–0.6 mm quartz sand ΔS on impact velocity v_0 : **a** – curve 1 – impact plate from WC-6Co hardmetal, $\alpha = 90^\circ$; curve 2 – the same as 1, $\alpha = 30^\circ$; curve 3 – impact plate from 0.2% C steel, $\alpha = 90^\circ$; curve 4 – the same as 3, $\alpha = 30^\circ$ and dependence of the increase in the specific surface of 0.3–0.4 quartz sand ΔS , on the hardness of collision surface HV : **b** – at impact velocity $v_0 = 120$ m/s: curve 1 – if $\alpha = 90^\circ$ and curve 2 – if $\alpha = 30^\circ$

Keeping in mind the service life (wear resistance) of mills working on the principle of collision, it is important to study what kind of materials used as impact members are most suitable for that purpose. The appropriate parameter in the analysis of the problem is the specific wear of the metal expressed as

$$K_g = I_g / \Delta S = (C_1 / C_2) v_0^{m-n}, \quad (2.2)$$

where K_g shows the wear of the material in mg per 1 m^2 of new surface generated.

There exist two alternative modes of obtaining the desirable grinding fineness, which differ in principle – either by a single impact at high velocity (*e.g.* in a jet mill), or by subsequent impacts at moderate velocity (*e.g.* in a disintegrator). It will depend on the ratio between the value of exponents m and n : if $m > n$ (in the case of steels without heat treatment) several impacts at moderate velocity are preferable. If $m < n$, however, (in the case of hardmetals and hardened steels in milling sand and glass at $v_0 = 150$ m/s, see Figures 1.17 and 1.18a), one impact at high velocity is preferable. It is illustrated in Table 2.2, in which the specific wear of metal when milling sand and cement clinker is shown [18].

Table 2.2. Specific wear of metal K_g , mg/m^2 by single impact milling, $\alpha = 90^\circ$

V_0 , m/s	Quartz sand		Cement clinker	
	0.2% C steel	WC-3Co hardmetal	0.2% C steel	WC-3Co hardmetal
75	11.5	0.15	4.7	0.13
150	15.5	0.11	6.7	0.09
325	24.7	0.09	10.5	0.05

The advantage of a hardmetal impact surface lies not only in a restricted specific wear of metal and increased operational reliability of the mill, but also in a considerable cutdown of energy consumption for milling. Relying on the data provided in Figure 14a, if, for example, $v_0 = 200$ m/s, and the grinding members are from steel, to obtain 1 m^2 of a new surface, 200 J of energy is required, whereas with hardmetal impact members only 114 J is necessary, *i.e.* 1.75 times less.

A phenomenon accompanying breakup of the particles is their adhesion to the surface. There are materials (from among metals, especially aluminum) in the initial stage of erosion of which the particles and their debris become mechanically attached to the surface. The latter takes place at large impact angles and, instead of loss in mass of the part, the growth of it initially occurs [4]. More typical, however, is molecular adhesion of the fragments forming during the impact to the surface owing to molecular power [5], which takes place at sufficiently high velocities. Figure 2.15 shows photos of adhesion to hardmetal surface, taken by means of a scanning electron microscope.

As it can be seen from Figure 2.15a, the central part of the impact scar of a spherical cast iron particle stays clean without any adhered splinters. The latter stay positioned on a concentric circle and resemble partially molten metal sprinkles. The diameter of the circle constitutes *ca* 60% of the initial diameter of the particle. The splinters adhered to the surface of irregular particles, however, are located rather irregularly.

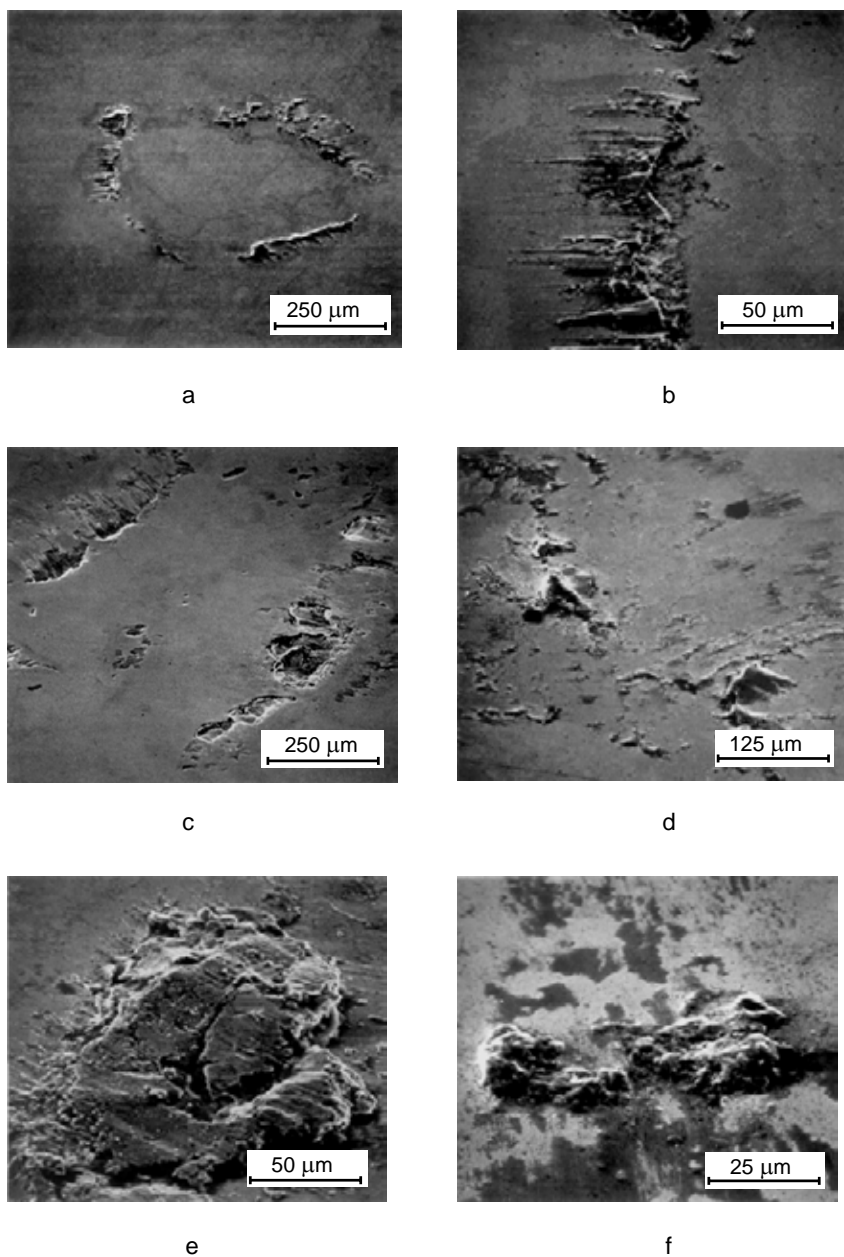


Figure 2.15a–f. Adhesion of 0.9 mm particle splinters to the surface of WC-6Co hardmetal in an impact at the velocity of 225 m/s, $\alpha = 90^\circ$: **a** – impact of a spherical cast iron pellet; **b** – an enlarged fragment of photo **a**, **c**, **d** – an impact with cast iron particle of an irregular shape; **e** – an enlarged fragment of photo **c**, **f** – impact of a quartz sand particle

2.4 References

1. Kleis I. About the erosion of metals in the jet of solid particles. Proc Techn Univ Tallinn 1959;168:3–27.
2. Langeberg I. Research into Abrasive Erosion at Low Impact Angles. PhD Thesis. Tallinn 1968 (in Russian).
3. Uuemõis H. Study of Some of Regularities Concerning Abrasive Erosion. PhD Thesis. Tallinn 1968 (in Russian).
4. Tadolder J. Abrasive Erosion of Technically Pure Metals. PhD Thesis. Tallinn 1966 (in Estonian).
5. Kleis I, and Uuemõis H. Untersuchung des Strahlverschleissmechanismus von Metallen. Zeitschrift für Werkstofftechnik. 5. Jahrgang. Heft 7, 1974;381–89.
6. Huthings IM, and Winter RE. The erosion of ductile metals by spherical particles. J Phys D. 1975; 8:8–14.
7. Huthings IM, Winter RE. and Field JE. Solid particle erosion of metals: The removal of surface material by spherical particles. Proc Roy Soc London 1976;A348:379–92.
8. Bogomolov NI. The processes occurring in contact of abrasive and metal. Proc of Symposium “Methods of Wear Testing”. Moscow: Publications of Academy of Sciences of USSR. 1962;12–18 (in Russian).
9. Saverin MM. Shot Peening. Moscow: Mashgiz Publishers, 1955 (in Russian).
10. Mosberg R, and Kleis I. The study of the processes taking place at the surface of metal at erosion. Proc Techn Univ Tallinn 1962;192:20–28 (in Russian).
11. Pakkas LR. Research into the Changes of Crystal Lattice in the Surface Layer of a Metal Target Subjected to Abrasive Erosion. PhD Thesis. Tallinn 1968 (in Russian).
12. Rinehart JS, and Pearson J. Behaviour of Metals Under Impulsive Loads.. Cleveland: Publ by The American Society for Metals 1954.
13. Olesevich KV. Wear of Elements of Gas Turbines Operating on Solid Fuel. Moscow: Mashgiz Publishers, 1959 (in Russian).
14. Uetz H, and Gommel G. Temperaturerhöhung und elektrische Aufladung beim Stoss einer Stahlkugel gegen eine Stahlplatte. Wear 1966;9:282–96.
15. Polosatkin GD, and Gribanov SA. The measurement of temperatures on cutter surfaces at velocities of 1 to 800 m/s. Inf Bull Higher Educ Inst, Phys;3: 1965, 173–175 (in Russian).
16. Kleis I, Muiste U, Pilvre U, Uuemõis H, and Uetz H. The physical mechanism of the formation of metal microspheres in the wear process. Wear 1979;58:79–85.
17. Reiners E. Der Mechanismus der Prallzerkleinerung beim geraden zentralen Stoss und die Anwendung dieser Beanspruchungsart bei der selektiven Zerkleinerung von spröden Stoffen. – Forschungsberichte des Landes Nordrhein-Westfalen nr. 1059, 1962.
18. Piel M. Study of the Laws Covering Wear and Grinding Processes in Impact Mills. PhD Thesis. Tallinn 1979 (in Russian).
19. Kleis I, and Uuemõis H. Wear Resistance of the Milling Equipment Operating on the Principle of Impact. Moscow: Mashinostroenie Publishing House, 1986 (in Russian).

Solid Particle Erosion

Occurrence, Prediction and Control

Kleis, I.; Kulu, P.

2008, XII, 206 p., Hardcover

ISBN: 978-1-84800-028-5